Designated ligand functionalization of gold nanoparticles for optimizing blue-phase liquid crystal composites

Kamil Orzechowski,[*1] Martyna Wasiluk,[2] Konrad Jabłoński,[1] Weronika Milewska,[1] Olga Strzeżysz,[3] Chun-Ta Wang,[4] Wiktor Lewandowski,[2] and Tomasz R. Woliński[1]

[1]*Faculty of Physics, Warsaw University of Technology, Koszykowa 75, 00-662 Warsaw, Poland*
[2]*Faculty of Chemistry, University of Warsaw, Pasteura 1, 02-093 Warsaw, Poland*
[3]*Institute of Chemistry, Military University of Technology, Kaliskiego 2, 00-908 Warsaw, Poland*
[4]*Department of Photonics, National Sun Yat-sen University, No. 70 Lien-hai Rd., Kaohsiung 80424, Taiwan*

Received December 08, 2024; accepted December 30, 2024; published December 31, 2024

Abstract—This work presents the impact of the composition of the organic shell of 4 nm gold nanoparticles (Au NPs) on the optical properties and stability of the nanoparticle-doped blue-phase liquid crystals (BPLCs). Particularly, we show that the binary shell of NPs, comprising LC-like ligands, can significantly enhance the thermal stability of BPs. Moreover, modifying the shell composition enables control over the Bragg wavelength of BPLCs. Our findings highlight the potential of ligand-functionalized Au NPs to optimize BPLC-based photonic devices, emphasizing ligand functionalization as a crucial factor for improving the stability of NPs and controlling BPLC properties.

Blue-phase liquid crystals (BPLCs) are emerging as a conspicuous class of materials in photonic technology. They exhibit properties such as fast electro-optical switching and have been tested in technologies ranging from detection to tuning and sensing. These highly chiral materials consist of liquid-crystalline molecules arranged into unique double-twist cylinders (DTCs), forming self-assembling three-dimensional (3D) stimuli-responsive soft crystals. BPLCs exhibit three thermo-sensitive mesophases: BP I, BP II, and an isotropic-like 'fog phase' BP III [1–2]. All three structurally distinct types of BPs appear in order of decreasing temperature from the isotropic to the cholesteric phase. Unfortunately, they naturally exist within a comparatively narrow temperature range (~0.1–5.0 °C), which propels research towards broadening the temperature range of BPs.

BPs I and II are particularly fascinating due to their cubic symmetry of molecular organization within the unit cell. BP I has a body-centered cubic lattice, where the lattice constant corresponds to the helical pitch. In contrast, BP II features a simple cubic lattice, with the lattice constant corresponding to half of the helical pitch. The structure of BPLCs gives rise to exceptional properties that can significantly enhance modern LC-based devices. These properties include 3D Bragg reflections, optical isotropy, sub-millisecond response times, and polarization insensitivity on a macroscopic scale for wavelengths outside their resonance bands [3–5]. However, a significant challenge is that they are stable within narrow temperature ranges. The structure of BPs can be seen as a defected structure of chiral nematic phases. Disclination lines arise between the DTCs, which impose low thermal stability on the BP. However, from the perspective of supramolecular chemistry, disclination lines, due to their higher entropy, become an interesting tool in the toolbox of nanotechnology. Namely, if BPs are doped with nano-objects, these nano-objects tend to assemble in the disclination lines. These regions make BPLCs a promising 3D template for doping with nanoparticles (NPs) (Fig. 1) and other nanomaterials. This doping process can create tunable BPLC composite materials with improved thermal stability, opening new possibilities for advanced photonic applications.

Numerous experimental studies have been aimed to enhance the thermal stability of BPLCs using various nanodopants, such as dielectric [6–7] and magnetic[8] NPs, carbon nanotubes [9], and graphene oxide [10]. Additionally, a few studies have focused on using NPs to tune the photonic properties of BPLCs, specifically by shifting selective light reflections [7], [11–12]. Typically, this shift moves towards longer wavelengths with higher NP concentrations, and its magnitude depends on the dielectric properties, dimensions, and shape of the NPs [13]. This phenomenon can be explained by the energetic penalty associated with disclinations, which drives the DTC structures apart, thereby enlarging the BP.

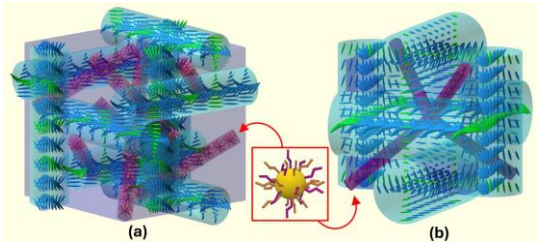

Fig. 1. Scheme of molecular ordering in cubic structures enriched with Au NPs, corresponding to a unit cell of (a) BP I and (b) BP II. Green molecules mean connected helices in neighboring double-twist cylinders, and violet rods correspond to an array of liquid-crystalline disclinations in a unit cell. The yellow sphere represents the Au core of

[*]E-mail: kamil.orzechowski@pw.edu.pl

NP, while orange and magenta curves correspond to different types of ligands.

unit cell beyond the equilibrium chiral twist. However, applying specific chemical functionalization to the NP surface (i.e., applied organic ligands) makes it possible to control the Bragg wavelength shift towards shorter wavelengths at higher NP concentrations in BPLC [12]. This effect occurs due to the interactions between specialized NP ligands with LC-like properties and LC molecules in DTCs or the chiral agents, which shorten the DTC helical pitch (i.e., increase the chiral twist) and reduce the BP unit cell size.

Since the revolution offered by the Brust-Schiffrin method for gold (Au) NP synthesis, the NPs used in composite materials research are typically coated with dodecanethiol (DDT) ligands – DDT molecules serve as stabilizers or growth-controlling agents during NP synthesis. These ligands' chemical stability prevents NP aggregation and endows NPs with hydrophobic (oleophilic) character, ensuring at least partial miscibility between NPs and systems such as LCs. However, the miscibility and stability of the formed mixtures are not consistently maintained, especially in LCs with more complex compositions and structures, like BPs. Thus, it is crucial to develop an understanding of the effect of ligand shell composition on the formation and stability of NP-LC materials and, hence, the properties of composite materials that go beyond the usual properties of LCs.

Here, we demonstrate that even a slight change in the organic shell of Au NPs can significantly affect the properties of BPLC and the stability of BPs. The transmission polarization microscopy method was used to observe the BPLC textures. Au NPs were used as dopants to BPLCs. The ligand shell comprised either DDT (unary type shell) or mixtures of DDT and LC-like ligands with varying ligand ratios (binary shell). The effects of varying NP ligand shells on BPLC were rationalized using small-angle X-ray diffraction (SAXRD) measurements of thin films made of Au NPs.

To prepare NP-doped BPLC composites, a mixture consisting of nematics 1912 (86 wt%) and two strongly twisting chiral dopants – biphenyl-4,4’-dicarboxylic acid bis- (1-methyl-heptyl) ester and [1,1';4',1'']terphenyl-4,4''-dicarboxylic acid bis-(1-methyl heptyl) ester (both 7%) were used. Each chemical component was synthesized at the Military University of Technology and described elsewhere [14–15]. The optical properties of all BPLC composites were examined in surface-treated flat cells (i.e., with homogeneously alignment layers applied, SE130, Nissan Chemical Industries, Ltd.) with a 12.0 ± 0.5 µm gap.

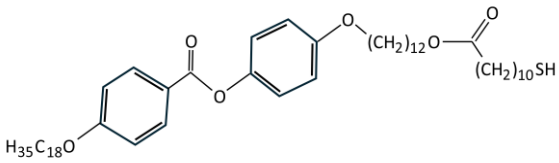

Fig. 2. A chemical formula of the used LC-like ligand.

Spherical Au NPs (4.0 ± 0.3 nm diameter), covered with four different organic shells, were used as nanoinclusions to BPLC. The NPs were prepared following a modified Brust-Schiffrin method, which yields NPs covered with the DDT coating [16]. Subsequently, for NPs with mixed ligand shells, DDT ligands were partially replaced in a ligand exchange reaction with an LC-like ligand. The chemical structure of LC-like ligands is presented in Fig. 2. Excess of unbound ligands used in the reaction was removed through multiple precipitation-centrifugation cycles[17], [18]. Au NPs with different mass ratios of DDT: LC-like ligands on the surface of the Au core were prepared as follows: 1:0 (Au@L1), 1:0.5 (Au@L2), 1:1 (Au@L3), and 1:2 (Au@L4).

BPLC samples were examined using polarized optical microscopy (POM) in transmission mode with crossed polarizers. Initially, POM images of BPLC textures were acquired for both pure organic and composite samples, the latter containing Au NPs at a concentration of 0.5% by wt. The BPLC samples were observed during slow cooling (at a rate of 0.2 °C/min) from the isotropic phase (ISO) through the blue phases (BPII, BPI) to the chiral nematic phase (N*). Cooling the BPLC samples formed BPs over a broader temperature range than heating, typically around twice as wide.

In the undoped sample, BP II exhibits selective reflection for red light, while BP I reflects blue/green light (see Fig. 3a). The thermal stability of these phases spans 3.5°C (54.5−58.0°C) for BP II and 2.0°C (58.0−60.0°C) for BP I. To investigate the impact of the organic shell composition around NPs on the formation of BPLC composites, we utilized Au NPs with varying mass ratios of binary ligands.

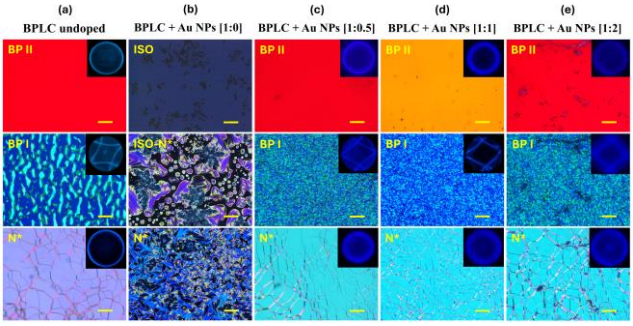

Fig. 3. POM images of BPLC composites enriched with NPs coated with ligands at different mass ratios of DDT: LC-like ligands. The insets show Kossel diagrams. Images were captured six months after doping

the BPLCs with the investigated NPs in transmission. The yellow bars represent a scale of 100 μm.

In the case of composites of BPLC and NPs, we initially examined a sample of BPLC doped with Au NPs coated with DDT ligands (Au@L1). This sample exhibited a pronounced tendency to separate the phase, forming dark islands of aggregated NPs noticeable in the ISO phase (see Fig. 3b). Upon cooling, the sample bypassed the formation of BPs, transitioning directly to a non-ordered N* phase with persistent NP aggregation, resulting in high light scattering.

We then focused on BPLC composite samples with Au NPs covered with the binary ligand shell. For Au@L2 NPs, it was observed that NPs do not alter the optical properties of BPLC compared to the undoped material (see Fig. 3c). In both BP II and BP I phases, the selective light reflection remains unchanged relative to the undoped BPLC. However, a decrease in the BP II-ISO phase transition temperature and an enhancement in the thermal stability of BP I were noted. Consequently, both BPs occurred within the following temperature ranges: 2.0°C (56.6−58.6°C) for BP II and 7.0°C (49.6−56.6°C) for BP I.

For the BPLC composite with Au@L3 NPs, a further decrease in the clearing temperature was noted, with both BP phases appearing within the following temperature ranges: 2.2°C (53.4−55.4°C) for BP II and 9.6°C (43.8−53.4°C) for BP I. Interestingly, a significant change in selective light reflection in BP II was observed, with a slight shift of the Bragg wavelength towards shorter wavelengths (see Fig. 3d).

At this stage, it is interesting to compare Au@L1 to composites with the binary shell (Au@L2 and Au@L3). Firstly, the presence of LC-like ligands enabled the efficient blending of the NPs with the BPLC. Namely, the lack of aggregates in the case of the binary shell can be attributed to the effect of LC-like ligands. As we have shown previously, with smaller NPs (2.4 nm diameter), such ligands facilitate mixing with the BPLC[12]. This is driven by the interactions between LC-like ligands and BPLC molecules, allowing the dispersion of particles within the BPLC volume. It has also been shown that LC-like ligands are equipped with molecular parts similar to those of the BPLC-forming compounds, such as aromatic rings and an elongated shape. Moreover, the binary-type shell enables the interdigitation of BPLC-forming molecules and the NP shell. However, doping the BPLC with an NP concentration of 5% wt. resulted in a substantial reduction in the unit cell lattice constant (up to ~14%), leading to a significant shift of the Bragg wavelength towards shorter wavelengths (by more than 80 nm), both changes observed for the BP I phase.

Finally, we prepared a BPLC composite with Au@L4 NPs in which the portion of LC-like ligands is the highest. In this case, no changes in selective light reflection were observed in either BP II or BP I phases compared to the undoped BPLC sample (see Fig. 3e). Surprisingly, the decrease in the clearing temperature was minimal compared to other examined BPLC composites with LC-like ligands coated on NPs. Additionally, a minute NP aggregation occurred after six months of the doped composite storage, visible as small dark spots, which reduced the sample's transparency. In the studied composite, BPs occurred within the following temperature ranges: 2.2°C (57.4−59.6°C) for BP II and 6.4°C (51.0−57.4°C) for BP I.

To thoroughly investigate the effect of doping with the selected Au NPs on the properties of the chiral structure lattice in BPs, we performed Kossel diagram measurements using a conoscopic microscopy setup, including a Bertrand lens and a microscope objective (60×, NA=0.7). Measurements were made for monochromatic light using a narrow bandpass optical filter (450 nm, FWHM=10 nm).

The collected Kossel diagrams confirm the presence of BP II (100) and BP I (110) phases, with the BP unit cells maintaining their orientation in each of the examined samples. When comparing the Kossel patterns of the undoped and doped (Au@L2) samples in BP I, we observed that the pattern sizes are identical (cf. Figs. 3a and 3c), indicating the formation of chiral structures with an identical lattice constant. However, for the doped (Au@L3) sample, the diagram size is significantly larger than that for the doped (Au@L2) sample, indicating a reduction in the BP I lattice constant and a shift in the Bragg wavelength towards shorter wavelengths (cf. Figs. 3a and 3d). Additionally, doping with the selected Au NPs may introduce some deviations from the established BP domain orientation, as evidenced by several Kossel patterns rotated relative to each other or blurred Kossel lines (see Figs. 3d and 3e).

Figure 4 offers a comprehensive comparison of all the studied BPLC cells. Two important conclusions can be drawn from these images. Firstly, the images highlight a shift in Bragg reflection in the N* phase due to NP doping with specific binary ligands. Compared to the undoped sample, the reflected light's different color confirms the Bragg wavelength change from orange to green induced by doping of Au@L1, Au@L3, and Au@L4. The change is most pronounced in the case of Au@L3 (compare Figs. 4a and 4d). Secondly, these images reveal the level of chemical compatibility of NPs to the BPLC. Namely, the dark spots in the BPLC cells with Au@L1 and Au@L4 NPs, which were recorded after six months of storage, suggest that these particles do not ensure full chemical compatibility with the investigated BPLC material (Figs. 4b and 4e). In the case of the BPLC sample with Au@L2 NPs, NP aggregation was not observed. However, partially darker areas in the BPLC cell appear, which can be ascribed to regions with higher NP content, suggesting reduced dispersibility of NPs within the LC (see Fig. 4c).

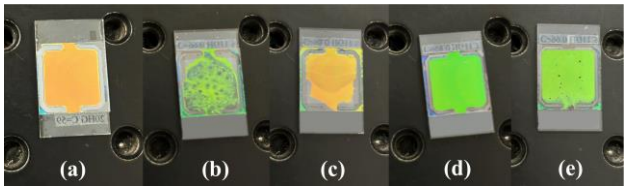

Fig. 4. BPLC cells undoped (a) and doped with Au NPs at different mass ratios of DDT:LC-like ligands on the NP shell: (b) 1:0, Au@L1, (c) 1:0.5, Au@L2, (d) 1:1, Au@L3, (e) 1:2, Au@L4. The presented images were recorded at room temperature, corresponding to the N* phase.

In contrast to all mentioned samples, the BPLC cell doped with Au@L3 NPs exhibits uniform selective light reflection. This indicates a uniform particle distribution and attests to chemical compatibility between NPs and the BPLC.

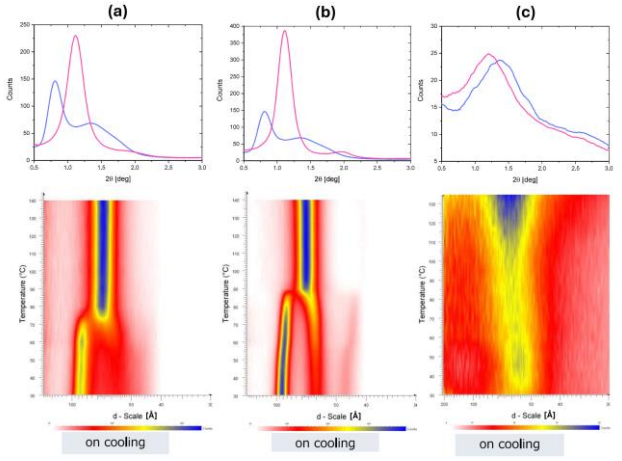

Fig. 5. Structural investigation of gold nanoparticles with binary ligands for (a) Au@L2, (b) Au@L3, and (c) Au@L4 NPs. The top panels illustrate the small angle X-ray diffraction (SAXRD) profiles for low (30°C, blue line) and high (120°C, magenta line) temperature structures. The bottom panels present a temperature evolution of SAXRD patterns on cooling.

Ultimately, the interaction efficiency between Au NPs and BPLCs strongly depends on the organic shell of the NPs. Varying amounts of binary ligands on the NP surface influence the properties of BPLC composites. This effect is driven by the structural properties of the NPs, which can be effectively investigated using the SAXRD method.

Figure 5 showcases the results of SAXRD pattern evolution measurements as a function of temperature for the analyzed Au NPs covered with the binary shells. It is worth noting that these particles can be divided into two categories. The first are Au@L2 and Au@L3 samples. These materials exhibit a switchable assembly; at low temperatures, they form a lamellar-type structure, while at elevated temperatures, they form an isotropic phase. Surprisingly, the positions of the main XRD peaks are very similar, evidencing that unit cell parameters are nearly identical. In the lamellar phase at 30°C, the inter-layer and in-layer distances are ~8.9 and ~6.2 nm for Au@L2, and ~9.2 and 6.1 nm for Au@L3, respectively. In the isotropic phase at 120°C, the mean center-to-center distance is ~6.4 for Au@L2, and ~6.5 nm for Au@L3 samples. These values were determined based on the maxima of the XRD signals relative to the d-Scale axis, expressed in Å, at appropriate temperatures from the bottom panels in Fig. 5. The slightly larger distances for Au@L3 are reasonable, given the relatively higher amount of bulky LC-like ligands in their shell than Au@L2. Nevertheless, the structural differences between the assemblies of Au@L2 and Au@L3 analyzed above can be considered relatively minor. The similar symmetry and interparticle spacing raise questions about the reasons for the conspicuous differences when doping BPLC with the Au@L2 and Au@L3.

We must look closer at the temperature-dependent XRD measurement results to answer this question. They reveal two significant differences in the structural behavior of Au@L2 and Au@L3 thin films.

Firstly, the Au@L3 sample exhibits more developed (narrow) XRD peaks, making both (01) and (02) signals visible, while no harmonics are visible in the case of Au@L2. In other words, the correlation length of particle assembly is longer for Au@L3. This suggests that the deformed organic shell of Au@L3 is more uniform compared to Au@L2. To fully appreciate the effect, it is worth noting that several previous works have shown that the lamellar phase of NPs forms due to the cylindrical/ellipsoidal shape of the binary organic shell of NPs. Namely, the LC-like ligands form bundles above and below the metallic sphere. These bundles determine the inter-layer distance, while the distance within the layers is determined by the thickness of the bundles and the length of the alkyl thiol ligands (here, DDT). Thus, looking from the perspective of molecular interactions, L3 coating seems to ensure efficient interactions of ligands (within a single particle and between particles) and efficient ligand interdigitation.

Secondly, the phase transition temperature (isotropic to lamellar) is significantly different: 75 and 90 °C, respectively, for Au@L2 and Au@L3 samples. Thus, Au@L3 samples favor the deformation of the organic shell.

Overall, the increased correlation length and higher phase transition temperature of Au@L3 can be ascribed to the features of the organic shell of NPs. Compared to Au@L2, Au@L3 NPs exhibit a higher deformation tendency and uniformity of the deformed organic shell.

Further, we analyze the SAXRD measurements of the Au@L4 sample. The most apparent difference between the Au@L2 and Au@L3 samples is that Au@L4 NPs do not form long-range ordered structures. At all tested temperatures, only a single-broad XRD signal is visible for Au@L4 thin films, which can be ascribed to an isotropic distribution of particles. Although the isotropic distribution spans over the tested temperature range, the

interparticle distance grows with the increase in temperature. This effect is expected for the growing entropic demand of LC-like ligands. The lack of the lamellar phase means that the organic shell of the particles does not tend to form a cylindrical/ellipsoidal shape. This effect is expected for NPs with a high loading of the LC-like ligands, leading to their steric crowding.

Overall, analyzing the above results, we may identify a few design factors of NP shell which seem relevant for efficient mixing with the BPLC and potentially influencing the stability of the BP phases:

(1) forming a binary organic shell that comprises LC-like ligands,

(2) ensuring a high tendency of the organic shell to (uniformly) deform.

Such a design seems to enable the efficient interactions of LC-like ligands with the molecules of BPLC and fitting into the disclination lines of BP phases.

In summary, this study demonstrates the significant impact of the organic shell of Au NPs on the optical properties and the chemical and thermal stability of BPLCs. By carefully selecting ligands on the surface of Au NPs, it is possible not only to enhance the stability of BPLCs but also might control the Bragg wavelength. The presented results reveal the potential for using Au NPs with functionalized surfaces in BPLCs as versatile materials, particularly for photonic technology applications.

This work was funded by the FOTECH-2 project of the Warsaw University of Technology within the Excellence Initiative: Research University (IDUB) program. K.O. would like to acknowledge support from the National Science Centre, Poland (MINIATURA UMO-2023/07/X/ST3/00943).

References

[1] S. Meiboom, M. Sammon, Phys. Rev. Lett. **44**, 13, 882 (1980).
[2] S. Tanaka *et al.* Sci. Rep. **5**, 1, 16180 (2015).
[3] W. Cao, A. Muñoz, P. Palffy-Muhoray, B. Taheri, Nat. Mater. **1**, 2, 111 (2002).
[4] H. Yoshida *et al.* Phys. Rev. E **94**, 4, 042703 (2016).
[5] K. Orzechowski *et al.* Opt. Mater. **69**, 259 (2017).
[6] H. Yoshida *et al.* Appl. Phys. Express **2**, 12, 121501 (2009).
[7] M.A. Gharbi *et al.* ACS Nano **10**, 3, 3410 (2016).
[8] W.-L. He *et al.* Phys. Chem. Chem. Phys. **18**, 42, 29028 (2016).
[9] A.P. Draude, T.Y. Kalavalapalli, M. Iliut, B. McConnell, I. Dierking, Nanoscale Adv. **2**, 6, 2404 (2020).
[10] M. Lavrič *et al.* J. Appl. Phys. **127**, 9, 095101 (2020).
[11] M. Ravnik, G.P. Alexander, J.M. Yeomans, S. Žumer, Proc. Natl. Acad. Sci. **108**, 13, 5188 (2011).
[12] K. Orzechowski *et al.* ACS Nano **16**, 12, 20577 (2022).
[13] U.N. Tohgha, E.P. Crenshaw, M.E. McConney, K.M. Lee, N.P. Godman, J. Colloid Interface Sci. **639**, 401 (2023).
[14] O. Chojnowska, R. Dąbrowski, J. Yan, Y. Chen, S.T. Wu, J. Appl. Phys. **116**, 21, 213505 (2014).
[15] P. Kula, J. Herman, O. Chojnowska, Liq. Cryst. **40**, 1, 83 (2013).
[16] M. Brust, M. Walker, D. Bethell, D J. Schiffrin, R. Whyman, J. Chem. Soc. Chem. Commun. **7**, 801 (1994).
[17] J. Grzelak, M. Żuk, M. Tupikowska, W. Lewandowski, Nanomaterials **8**, 3, 147 (2018).
[18] M. Bagiński *et al.* ACS Nano **15**, 3, 4916 (2021).

